Live Cell NMR

Darón I. Freedberg[1] and Philipp Selenko[2]

[1]Laboratory of Bacterial Polysaccharides, Center for Biologics Evaluation and Research, U.S. Food and Drug Administration, Rockville, Maryland 20852-1448; email: daron.freedberg@fda.hhs.gov

[2]In-Cell NMR Laboratory, Department of NMR-Supported Structural Biology, Leibniz Institute of Molecular Pharmacology (FMP Berlin), 13125 Berlin; email: selenko@fmp-berlin.de

Annu. Rev. Biophys. 2014. 43:171–92

The *Annual Review of Biophysics* is online at biophys.annualreviews.org

This article's doi: 10.1146/annurev-biophys-051013-023136

Keywords

in-cell NMR, on-cell NMR, in-cell EPR, macromolecular crowding, excluded volume, soft interactions

Abstract

Ever since scientists realized that cells are the basic building blocks of all life, they have been developing tools to look inside them to reveal the architectures and mechanisms that define their biological functions. Whereas "looking into cells" is typically said in reference to optical microscopy, high-resolution in-cell and on-cell nuclear magnetic resonance (NMR) spectroscopy is a powerful method that offers exciting new possibilities for structural and functional studies in and on live cells. In contrast to conventional imaging techniques, in- and on-cell NMR methods do not provide spatial information on cellular biomolecules. Instead, they enable atomic-resolution insights into the native cell states of proteins, nucleic acids, glycans, and lipids. Here we review recent advances and developments in both fields and discuss emerging concepts that have been delineated with these methods.

Contents

DEDICATION

This review is dedicated to the memory of Flemming Martin Poulsen (F.M.P.). When asked to name which mammalian protein was natively present at the highest intracellular concentration (29, 30), students at a recent summer school on the Greek island of Spetses were speechless. A gentleman in the front row smiled and eventually provided the correct answer: hemoglobin in red blood cells at ~5 mM (96). The reason why this man knew the answer became evident only later. He was the late Flemming Martin Poulsen, the long-term organizer of the school and an eminent figure in early nuclear magnetic resonance (NMR) work on intact cells. As a postdoctoral scholar with Chris Dobson, then at Harvard University, Flemming spent much of his time measuring one-dimensional (1-D) ^{31}P, ^{1}H, and ^{19}F NMR spectra of different blood cells (20, 21), often his own, and he knew their protein compositions very well. As he said later, 1-D NMR experiments on intact red blood cells revealed the characteristic hemoglobin envelope known from previous NMR work on the isolated protein (93). These experiments, he added, may therefore be considered the first high-resolution in-cell NMR measurements. "Since we recorded on NMR spectrometers of less than 300 MHz field strengths, used primitive pulse sequences (compared to modern standards) and isotope detection at natural abundance," Flemming said, "what delight it must be to do in- and on-cell NMR experiments on modern instruments with advanced, multidimensional pulse-schemes and isotope-labeled samples!" He was absolutely right.

INTRODUCTION

Underlying most in- and on-cell nuclear magnetic resonance (NMR) applications today is an elegant and startlingly simple concept: isotopic labeling. With it, we exploit the fact that isotope-labeled, NMR-visible biomolecules stand out in unlabeled, NMR-inactive environments. The isotope thereby functions as a selective visualization filter that enables the detection of structural and functional properties of labeled biomolecules against the backdrop of all unlabeled cellular components. In that sense, in- and on-cell NMR applications work in much the same way as fluorescence microscopy. Fluorescence microscopy probes must be chemically attached, expressed as green fluorescent protein (GFP) fusions, or tagged via fluorescence-conjugated antibodies. Samples detected with in- or on-cell NMR methods are made visible by selectively replacing certain atomic nuclei with stable, NMR-active isotopes. Therefore, the actual label

is a quantum mechanical rather than a chemical property. Biomolecules studied with in- or on-cell NMR methods contain only natural components that are slightly heavier than their endogenous counterparts. This is an important aspect of in- and on-cell NMR methods, as all other cell-based visualization techniques require some form of target modification for detection. Because isotope-labeled biomolecules need to be selectively enriched or delivered into cells, key aspects of live cell NMR applications concern the actual sample preparation process.

IN-CELL NMR IN PROKARYOTES

In most cases, isotopic labeling of recombinant proteins is achieved in *Escherichia coli*. Bacteria are grown in media containing ^{15}N-ammonium chloride, ^{13}C-glucose, or D_2O as the only source of metabolic precursors. Upon induction of recombinant protein expression, ^{15}N-, ^{13}C-, or ^{2}H-isotopes are incorporated into the newly synthesized polypeptides. For general in- and on-cell NMR experiments in prokaryotes and for in-cell NMR applications in yeast, insect, and mammalian cells, overexpressed proteins are directly analyzed inside the expression host (87) (**Figure 1*a***). Because bacterial T7 expression systems yield remarkably high levels of intracellular proteins, isotope-labeled specimens can be rapidly generated.

In practice, unlabeled growth media are substituted with isotope-labeled media shortly before induction (87). Because T7-dependent, recombinant protein production outperforms endogenous protein synthesis, plasmid-encoded polypeptides constitute the only isotope-labeled species in the cells. When recombinant protein expression levels are high, the resulting in-cell NMR spectra are virtually free of background labeling artifacts. Protein overexpression, isotopic labeling, and NMR measurements in the same cellular system provide advantages and disadvantages. On the positive side, bacterial in-cell NMR samples are prepared quickly (90), and, provided that isotope-labeled proteins tumble freely in the cytoplasm and do not overly interact with cellular components such as membranes, in-cell NMR detection by solution-state methods is straightforward. Whenever target proteins are inserted into membranes, solid-state in- or on-cell NMR approaches are more suitable and are usually chosen (74). On the negative side, recombinant protein production is difficult to control, and absolute intracellular protein concentrations are hard to quantify and reproduce precisely. Intracellular protein solubility may also negatively affect in-cell NMR results. Because large amounts of recombinant proteins often lead to intracellular aggregation and precipitation, bacteria package excess proteins into inclusion bodies, which is deleterious for solution-state in-cell NMR efforts but amenable to solid-state NMR approaches (24, 102). If, however, recombinant protein expression levels are low and lengthy induction times are required to reach sufficient amounts of intracellular protein, decreased cell viability and increased background labeling often hamper in-cell NMR analyses.

IN-CELL NMR IN EUKARYOTES

The bacterial rationale of sample overexpression, isotopic labeling, and in-cell NMR measurements within the same cell type, which, until recently, was not considered a viable option for in-cell NMR sample generation in eukaryotes, has now been achieved in yeast (16), insect (33), and mammalian cells (11, 12) (**Figure 1*b–d***). The Shekhtman group (16) used *Pichia pastoris* and controlled methanol induction under the strong alcohol oxidase gene 1 promoter (AOX1) to produce yeast in-cell NMR samples, whereas the Ito, Shirakawa, and Laue laboratories (33) employed baculovirus-transfected Sf9 cells for in-cell NMR applications in insect cells. The Aricescu and Banci groups (11, 12) generated mammalian in-cell NMR samples by transient protein overexpression and isotopic labeling in human embryonic kidney HEK293T cells driven by the cytomegalovirus (CMV)

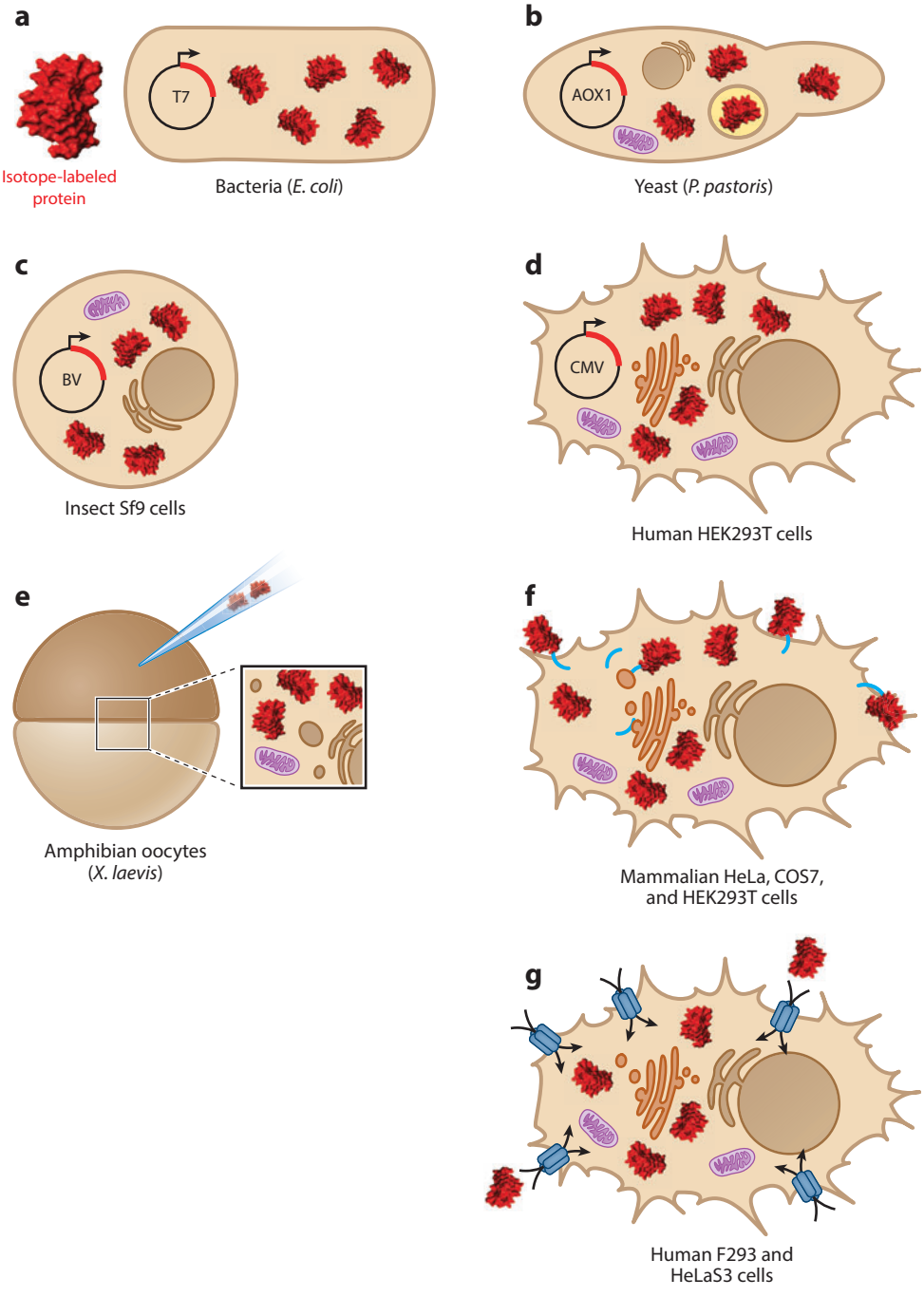

promoter. Despite these strong promoters, protein expression and labeling times were generally longer than in bacteria and led to substantial degrees of background labeling. For insect and mammalian in-cell NMR samples, costly commercial isotope-labeling media were used. Whereas Sf9 cells are nonadherent suspension cells that can be grown in small batch volumes, human HEK293T grow as single-layer cultures and require larger volumes of isotope-labeled growth media. Because all of the above methods rely on plasmid- and strong promoter–driven protein overexpression coupled to induction time–matched isotopic labeling, they exclusively enable the production of protein in-cell NMR samples.

Alternatively, isotope-labeled biomolecules may be first produced in *E. coli*, purified, and then introduced into eukaryotic cells. Sample delivery can be accomplished by microinjection, as for in-cell NMR applications in *Xenopus laevis* oocytes (1, 17, 81, 82, 85, 86) (**Figure 1*e***); by active endocytotic transport via the use of cell-penetrating peptide (CPP) tags (25, 42); or by passive diffusion through pore-forming toxins (52, 71) (**Figure 1*f*,*g***). The latter approaches are usually employed to transduce proteins into cultured mammalian cells. Two of the many advantages of sample production and isotopic labeling in one cell type and in-cell NMR measurements in another are that background labeling artifacts are not encountered and that DNA and RNA can also be delivered for in-cell NMR and electron paramagnetic resonance (EPR) studies (8, 36–38, 40, 51).

SOLUTION-STATE IN-CELL NMR

In the following section, we review recent solution-state in-cell NMR applications that delineate fundamental physical properties of the intracellular environment and provide unexpected clues for complex cellular processes. The selection does not reflect a weighting of scientific importance, quality, or impact. Instead, we provide a level of thematic coherence by discussing in-cell NMR studies from different groups either on identical proteins in different intracellular environments or on the same biological topic. We further limit the review to in-cell NMR studies that have not been previously reviewed (43, 55, 62, 73). We apologize in advance to our colleagues whose work is not included in this selection.

In-Cell Protein Structure, Dynamics, and Stability

A number of recent solution-state in-cell NMR applications aimed to provide a more detailed understanding of the physicochemical parameters that shape the intracellular environment and how they affect the folding, structure, dynamics, and stability of proteins inside cells. General physical properties of the intracellular environment, such as high degrees of macromolecular crowding, excluded volume effects, and increased overall viscosity (29, 30, 68, 69), were identified early on as disadvantageous for in-cell NMR experiments on large, folded proteins (89). However, several studies defied the notion that protein size alone determined the quality of in-cell NMR

Figure 1

Overview of prokaryotic and eukaryotic in-cell NMR systems. (*a*) Accumulation of isotope-labeled protein inside *Escherichia coli* by T7 promoter–driven overexpression. (*b*) AOX1-driven protein production in the yeast *Pichia pastoris*. (*c*) Baculovirus (BV)-infected insect Sf9 cells. (*d*) Cytomegalovirus (CMV) promoter–driven protein overexpression and isotopic labeling in human HEK293T cells. (*e*) Delivery of isotope-labeled proteins by microinjection into *Xenopus laevis* oocytes. (*f*) Transduction of cell-penetrating peptide (CPP)-tagged (*cyan*) cargo proteins into cultured mammalian cells. (*g*) Delivery of isotope-labeled proteins into mammalian cells through bacterial pore-forming toxins (*blue*). Cells not drawn to scale.

spectra. Below, we discuss experiments that illuminated the nature of some inherent protein properties driving in-cell NMR behaviors.

Our first example is the B1 domain of the streptococcal protein G (GB1), which has served the in-cell NMR community as a reliable gold standard ever since its astounding in-cell NMR qualities were reported in *X. laevis* oocytes (86). GB1 is a 56-residue, folded protein domain that is highly negatively charged [~6.2 kDa, isoelectric point (pI) 4.2] and is often considered biologically inert. All GB1 in-cell NMR spectra collected thus far in different cell types have been of excellent quality. By contrast, ubiquitin (Ub), a similarly small, 76-residue folded protein (~8.6 kDa, pI 5.7) yielded in-cell NMR spectra of varying quality. Whereas Burz et al. (18) obtained in-cell NMR spectra in *E. coli*, many other groups were unable to do so (13, 57, 100). In higher eukaryotic cells, in-cell NMR signals of wild-type Ub were equally difficult to detect, whereas a Ub mutant with alanine substitutions at three conserved surface residues (i.e., Ub-3A) produced reasonable in-cell NMR spectra (42, 82). In bacteria, the same Ub-3A mutant failed to yield in-cell NMR signals (100). Once again, the Shekhtman laboratory (16) delivered the exception to the rule by reporting decent quality in-cell NMR data on wild-type Ub inside the yeast *P. pastoris*. This time, though, they used the heterologous *Saccharomyces cerevisiae* isoform of Ub, which has a more neutral net charge (~8.5 kDa, pI 7.3). Upon cell lysis, most groups detected good-quality Ub or Ub-3A NMR signals in crude cell extracts, thus indicating that severe in-cell line broadening was not caused by stable interactions with cellular components.

Wang et al. (100) realized that a double GB1 construct containing two concatenated domains (~12.5 kDa, pI 4.4) produced excellent in-cell NMR spectra, whereas a GB1-NmerA fusion yielded sharp GB1 signals and severely line-broadened NmerA resonances (NmerA: ~6.9 kDa, pI 7.2). After cell lysis, uniform NMR signals of both domains were detected. Along the same lines, Crowley et al. (22) comparatively analyzed the bacterial in-cell NMR behavior of GB1 and several cytochrome *c* (Cyt *c*) variants (~12.2 kDa, pI 9.8). Wild-type and mutant Cyt *c* with substitutions of positively charged residues that reduced the net charge state from 9.8 to 8.2 (i.e., Cyt *c*-R13E/K73E/K87E) were not detected inside cells. When the authors separated crude cell extracts of these in-cell NMR samples by size-exclusion chromatography, they found that only GB1 eluted according to its molecular weight, whereas all forms of Cyt *c* were retained in high-molecular-weight fractions. These results suggested that Cyt *c* interacted with endogenous components of the *E. coli* cytoplasm, which in turn may have negatively affected its in-cell NMR properties.

What factors determine whether a protein engages in intracellular interactions? The most important is probably its biological activity. Ub, for example, executes a plethora of biological functions in organisms of all phyla, and most of these functions are mediated by interactions with other cellular proteins. Therefore, Ub is poised to engage in multiple interactions inside cells that probably also scavenge nonphysiological amounts of overexpressed protein. Poor quality in-cell NMR spectra are likely to result from such interactions. Analogously, the biological activity of the DNA-binding protein MetJ hampers its in-cell NMR detection through nonspecific interactions with cellular DNA (4). Similar effects are expected for many other proteins that engage in generic interactions with cellular components, especially when their respective binding partners are overly abundant in the cytoplasm. Unsuccessful, and therefore unpublished, in-cell NMR attempts with different WW and SH3 domains binding to proline-rich protein sequences bear silent witness to this notion.

Other proteins such as Cyt *c* may engage less overtly in specific interactions but exhibit surface charge properties that predispose them to nonspecific binding events. Indeed, Cyt *c* uses a highly positively charged surface area to interact with two coenzymes, Cyt *c* reductase and oxidase. Because both coenzymes are absent from the cytoplasm of *E. coli*, this surface area is likely to attract a multitude of unspecific electrostatic interactions. Indeed, when Crowley et al. (22) increased

the salt concentration in their cell extracts, wild-type and mutant Cyt *c* eluted at smaller molecular weight fractions. Despite these salt-dependent reductions of nonspecific Cyt *c* interactions, severe line broadening persisted in *E. coli* lysates. Only NMR signals of the most charge-reduced Cyt *c* mutant were detected (22). These data indicate that in addition to biological interactions, nonspecific electrostatic contributions also affect the quality of in-cell and lysate NMR spectra. Large positive net charges in particular are detrimental to in-cell NMR studies because of the abundance of negatively charged biomolecules in any cellular environment [e.g., proteins, nucleic acids (NAs), and phospholipids]. More than 70–90% of *E. coli* proteins are acidic or neutral with pI values between 4 and 7, which strongly suggests that their surfaces are anionic at physiological pH (59, 97). This in turn may ensure that nonspecific electrostatic contacts are kept to a minimum so as not to interfere with viable cellular functions that depend on unrestricted protein motions in the cytoplasm.

In contrast to GB1, Ub, and Cyt *c*, NmerA is uncharged at physiological pH. Nevertheless, its in-cell NMR spectrum displays significantly broadened resonances as compared to GB1 (100). Why does NmerA yield poor in-cell NMR spectra? We allude to cellular interactions of biologically active Ub as a possible reason for its poor in-cell NMR performance and list positive charges on the surface of Cyt *c* as mediating weak electrostatic interactions with generic cellular components that similarly debilitate its in-cell NMR behavior. In the case of NmerA, Wang et al. (100) and others (26, 39) argue that hydrophobic surface properties constitute yet another physical parameter that determines the overall stickiness of proteins inside cells (i.e., their tendency to interact with cellular components). Whereas hydrophobic residues are usually buried in the core of a folded protein, NmerA exposes a disperse set of aliphatic amino acids on its surface. This may account for its poor in-cell NMR behavior. In a striking analogy, exposed hydrophobic residues that facilitate protein-protein interactions also mediate the biological activity of wild-type Ub. In the better behaved Ub-3A mutant, alanines replace these hydrophobic residues. Therefore, surface hydrophobicity, protein stickiness, and biological activity may well be interconnected.

Interestingly, NmerA was the first protein to be studied by solution-state in-cell NMR spectroscopy, and experiments in 2001 yielded high quality in-cell NMR spectra (88, 89). When the same protein was reanalyzed under presumably identical conditions about 10 years later, its spectral quality was poorer than that of the original sample (100). What happened? One possible explanation is a difference in intracellular protein levels. If nonspecific hydrophobic contacts impeded the quality of NmerA in-cell NMR spectra, did higher intracellular protein levels promote NmerA binding to itself? In other words, did recombinant protein overexpression exacerbate the problem of nonspecific protein-protein interactions? Pielak and colleagues (95) asked this question in 2009. In their experimental setup, these authors used GFP (~27 kDa, pI 5.8) and fluorescence-based readouts of in-cell GFP diffusion to measure changes in intracellular stickiness upon co-overexpression of four additional proteins: maltose-binding protein (~42 kDa, pI 4.9), tau (~45 kDa, pI 7.5), α-synuclein (~14 kDa, pI 4.5), and calmodulin (CaM, ~17 kDa, pI 3.9). The authors found no detectable differences in intracellular GFP diffusion, suggesting that the presence of large amounts of recombinant proteins did not impede intracellular protein movements on a macroscopic scale.

What happens on the microscopic scale? Can enhanced hydrophobic interactions modulate the structure of a protein? To address this question, the Pielak group (84) employed a variant of the immunoglobulin G binding domain of protein L (ProtL) from *Streptococcus magnus* (wild-type ProtL, ~7 kDa, pI 4.5) with lysine to glutamic acid substitutions at seven positions (i.e., Kx7E, pI 3.1). In contrast to wild-type ProtL, 84% of the Kx7E variant is disordered in solution under low salt conditions. Differences in nonpolar side-chain solvation (i.e., the substituted amino acids), rather than an increase in overall negative charge, cause these changes (98). Kx7E folding

can be triggered in vitro by higher salt concentrations. The unfolding free energy of Kx7E is −1.0 kcal/mol, which corresponds to a small energy difference between the folded and disordered protein states. This means that the protein may easily unfold or may be present in solution as an equilibrium mixture between the folded and unfolded states. Macromolecular crowding theory predicts that chemically inert, hard-sphere repulsions stabilize folded proteins and promote folding of disordered proteins by minimizing excluded volume effects (68, 69). Would hard-sphere repulsions in the *E. coli* cytoplasm induce folding of Kx7E, according to macromolecular crowding theory, or would different types of weak intracellular interactions—appropriately termed soft interactions by Pielak's group (65, 83)—dominate over hard-sphere repulsions and preserve the disordered state (70), as experiments on other proteins have shown (15, 66, 67, 101)?

Despite its highly acidic nature, small size, and structural similarity to GB1, overexpressed ProtL did not yield interpretable in-cell NMR spectra, although it was easily detected upon cell lysis (84). By contrast, good quality in-cell NMR spectra of Kx7E were obtained, and their characteristics showed that the variant remained disordered in the cytoplasm of intact cells. Increasing the salt concentration from ∼0.2 M to ∼0.5–0.9 M in vitro induced Kx7E folding, whereas a similar increase did not induce folding in cells. These results established that hard-sphere repulsions were not sufficient to fold Kx7E in vivo and that soft interactions preserved the disordered protein state, even under conditions that promoted folding in vitro (84).

Latham & Kay (53, 54) investigated the effects of soft interactions on the side-chain dynamics of Calmodulin (CaM) in crude bacterial cell lysates (14). They prepared differentially ^{13}C-methyl-labeled CaM in its apo-, holo-, and peptide-bound states [i.e., in complex with smooth muscle myosin light chain kinase peptide, CaM-smMLCK(p), ∼20 kDa, pI 4.3]. The structures of these three versions of CaM also differ substantially. Whereas the folded N- and C-terminal domains of apo-CaM are flexibly connected via a disordered linker region, Ca^{2+} binding rigidifies this linker and induces the formation of a stable α-helix. This forces holo-CaM into a globally extended, dumbbell-shaped structure. Concomitantly, side-chain methyl groups that are buried in apo-CaM become solvent-exposed. This topology enables smMLCK(p) binding, upon which holo-CaM tightly wraps around the ligand in a globular conformation, again shielding its hydrophobic residues from the solvent. These three structural states also differ in the two-dimensional (2-D) ^{1}H-^{13}C correlation spectra of their methyl groups.

Latham & Kay (53) first exploited these discriminatory features to comparatively analyze the dynamic properties of selectively isotope-labeled CaM in vitro and in cell lysates. Starting with Ca^{2+}-free apo-CaM, they established that the amplitude and time scale of pico- to nanosecond side-chain motions were very similar in aqueous solution and cell lysates. By contrast, greatly attenuated microsecond-timescale motions of apo-CaM were detected in *E. coli* extracts. To further characterize these modulations, the authors performed Carr-Purcell-Meiboom-Gill (CPMG) relaxation dispersion experiments to probe for differences in millisecond-timescale motions. They detected substantial degrees of conformational exchange, which were likely caused by transient side-chain interactions with cellular metals, as lysate EDTA complexation and in vitro metal titration experiments suggested.

The overall spectral quality of Ca^{2+}-loaded CaM in bacterial cell lysate was considerably poorer and revealed significant line broadening. Indeed, the greater exposure of hydrophobic surface areas in Ca^{2+}-CaM indicated that nonspecific hydrophobic interactions with cellular components accounted for these line broadening effects. Lysate CPMG relaxation dispersion profiles were greater than those of apo-CaM and also pointed to different protein residues being affected by exchange contributions, such as the Ca^{2+}-CaM methionines involved in substrate binding. Latham & Kay (53) interpreted this behavior as a frustrated ligand search resulting in weak, short-lived interactions with components of the bacterial cytoplasm. If nonspecific soft interactions were

indeed to cause these effects, then binding to a high-affinity CaM ligand should reduce line broadening. In support of this hypothesis, the authors measured markedly improved signal intensities of ligand-complexed CaM-smMLCK(p) in cell lysates reminiscent of apo-CaM. Additional CPMG experiments indicated that millisecond-timescale motions and exchange contributions had essentially vanished.

In summary, these data substantiated the notion that different soft interactions, ranging from transient metal binding to frustrated hydrophobic searches, affected CaM's side-chain dynamics and, in turn, its spectral quality in bacterial cell lysates. They thus provided compelling experimental evidence that differences in lysate NMR behaviors resulted as a direct consequence of CaM's structural and functional properties (53).

In a follow-up study, the same authors characterized the strengths of these nonspecific interactions using lysate titration experiments (54). They measured changes in CaM methyl chemical shifts as a function of added *E. coli* extract to determine average minimum dissociation constants with endogenous lysate components. These lysate K_D values were in the low millimolar range (~0.22 mM), which is in good agreement with previous estimates for cellular NmerA interactions in intact bacteria (tens of millimolar) (100) and for nonspecific interactions of truncated chymotrypsin inhibitor 2 (~7.2 kDa, pI 9.0) with bovine serum albumin as an in vitro crowding agent (~35 mM) (67).

In-Cell Maturation and Metal Binding of Human Superoxide Dismutase 1

Human superoxide dismutase1 (hSOD1) is a 16-kDa protein (pI 5.9) that binds one Zn^{2+} atom at its structural metal binding site and one Cu^{2+} atom at its catalytic site. Disulfide bond formation and dimerization entails hSOD1 maturation (i.e., holo-hSOD1). The protein localizes to the cytoplasm and intermembrane space of mitochondria, where it is primarily responsible for clearing reactive oxygen species such as free superoxide radicals to maintain mitochondrial and thereby cellular homeostasis. Misfolding of apo-hSOD1 during individual steps of the maturation process has been implicated in many familial forms of amyotrophic lateral sclerosis, also called Lou Gehrig's disease, a major neurodegenerative disorder that leads to fatal motor neuron impairments.

The structural, dynamic, and topological folding properties of hSOD1 in its various maturation steps have been extensively studied in vitro, but high-resolution insights into these processes in cells were missing until recently. Banci et al. (10) were the first to use bacterial in-cell NMR to study the structural properties of apo-hSOD1 in *E. coli*. Upon protein overexpression and ^{15}N isotope labeling in metal-free medium, 2-D spectra revealed strong but poorly dispersed NMR signals of hSOD1 that superimposed well with the unfolded portions of the metal-free, monomeric, and reduced protein observed in in vitro NMR experiments (i.e., E,E-hSOD1^{SH-SH}, where E denotes empty metal-binding sites and SH–SH reduced cysteines). Such strong in-cell NMR signals of unfolded protein regions and selective line broadening of folded parts of a protein typically point to faster internal dynamics and more favorable relaxation properties of disordered protein regions than of folded protein domains, whose relaxation properties are determined by their overall correlation time, τ_c (13, 55). Weak resonances of the folded portions of E,E-hSOD1^{SH-SH} were detected at NMR chemical shift values similar to those seen in in vitro experiments. When bacteria were lysed and the cell slurry directly analyzed by NMR, the peak intensities of NMR signals in all spectral regions increased considerably due to decreased viscosity and greater overall tumbling. Even the folded portions of E,E-hSOD1^{SH-SH} displayed signal intensities and peak positions similar to those from in vitro NMR experiments, suggesting that hSOD1 retained its partially folded in vitro characteristics in *E. coli* cells and did not scavenge free metals in the bacterial cytoplasm (i.e., the protein remained in its metal-free apo-state). Peak positions of cysteine residues further confirmed the preservation of their reduced states.

When the authors recorded in-cell NMR spectra of apo-SOD1 in the presence of different amounts of external Zn^{2+} (ranging from substoichiometric 10 μM to superstoichiometric 1 mM), they detected all major NMR characteristics of the metal-bound E,Zn-hSOD1^{SH-SH} protein (10). Surprisingly, however, in-cell NMR signal intensities of folded and unfolded residues in E,Zn-hSOD1^{SH-SH} were greater than those of apo-SOD1 in the previous in-cell NMR samples, which challenged the notion that differences in protein dynamics alone accounted for the observed line-broadening effects. By excluding contributions from oligomerization or aggregation, Banci et al. (10) reasoned that nonspecific soft interactions with components of the bacterial cytoplasm caused the weak signal intensities of apo-SOD1. In-cell NMR signals also revealed that the second metal binding site remained unoccupied in E,Zn-hSOD1^{SH-SH}. The authors noted that, in vitro, the addition of equimolar amounts of Zn^{2+} to apo-hSOD1 leads to the formation of mixed populations of E,Zn-hSOD1^{SH-SH} and Zn,Zn-hSOD1^{SH-SH}, whereas further addition of Zn^{2+} produces uniform Zn,Zn-hSOD1^{SH-SH}. These findings were in stark contrast to their in-cell NMR results in the presence of excess amounts of Zn^{2+}. Only upon cell lysis and extract NMR measurements did Banci et al. (10) detect the formation of Zn,Zn-hSOD1^{SH-SH}.

These data argue that inside *E. coli*, a highly effective regulatory mechanism ensures the selectivity of the metal binding reaction and prevents loading of the Cu^{2+} site with excess Zn^{2+}. One explanation for the observed behavior was direct surveillance of intracellular Zn^{2+} levels by the bacteria, ensuring that only high affinity Zn^{2+}-binding sites were loaded with the metal and that metal-selective bacterial pumps actively extruded excess free ions from the cytoplasm. Alternatively, E,Zn-hSOD1^{SH-SH} may have existed in intracellular conformations that prevented additional metal binding, or it may have interacted loosely with cellular components that mediated such effects. Indeed, several cross-peaks of in-cell or lysate hSOD1 did not superimpose with in vitro reference spectra of free E,Zn-hSOD1^{SH-SH}, probably indicating additional cellular interactions. Yet other scenarios involve partial disulfide bond formation, or cysteine oxidation, prior to second metal binding, which could have occurred upon cell lysis. Banci et al. (10) did not analyze the in-cell NMR behavior of Cu^{2+} binding at that point because gram-negative bacteria such as *E. coli* contain very little free cytoplasmic Cu^{2+} and have efficient efflux pumps to remove intracellular copper.

In a breakthrough attempt to study hSOD1 maturation in intact human cells, Banci et al. (11) developed a new protocol for sample overexpression, isotope labeling, and in-cell NMR measurements in cultured embryonic kidney HEK293T cells. In the absence of exogenous metals in the growth media, they observed E,E-hSOD1^{SH-SH} with NMR characteristics similar to those in bacterial cells, i.e., intense NMR signals of unfolded apo-SOD1 regions and selective line broadening of folded parts of the protein. Trace amounts of uncomplexed Zn^{2+} led to the formation and detection of small amounts of E,Zn-hSOD1^{SH-SH}. When growth media were supplemented with Zn^{2+}, apo-hSOD1 was efficiently converted into E,Zn-hSOD1^{SH-SH}, which similarly yielded high quality in-cell NMR spectra. This indicated that, similar to *E. coli*, Zn^{2+} was efficiently taken up by mammalian cells and selectively bound to one of the metal sites of apo-hSOD1.

At this point, the authors revisited their *E. coli* in-cell NMR system to comparatively investigate the binding behavior of copper (11). When Zn^{2+} and Cu^{2+} salts were added to the bacterial growth medium, in-cell NMR experiments of ^{15}N isotope-labeled hSOD1 reported the reduction of Cu^{2+} to Cu^{+} and the formation of mixed Cu,Zn-hSOD1^{SH-SH} and Cu,Zn-hSOD1^{S-S} species. This showed that in the bacterial cytoplasm, intracellular hSOD1 bound copper, which coincided with partial disulfide bond formation. Interestingly, the direct addition of Cu^{+} salts to the growth medium did not result in copper binding. When hSOD1 loading with copper was studied in mammalian cells, only ~25% of intracellular E,Zn-hSOD1^{SH-SH} bound the metal in its Cu^{+} state, whereas ~75% remained copper-free. Accordingly, only ~20% of hSOD1 formed disulfide bonds.

Because eukaryotic copper homeostasis is tightly controlled at multiple levels and efficient hSOD1 copper loading requires the activity of the copper chaperone for SOD1 (CCS) protein, Banci et al. (11) co-overexpressed and isotopically labeled hSOD1 and CCS in HEK293T cells. In the presence of Cu^{2+} salts, in-cell NMR experiments showed a higher ratio of copper/zinc- to zinc-bound hSOD1 (1:1), supporting the notion that CCS promoted copper incorporation. In addition, they observed efficient formation of disulfide bonds, which was further stimulated by Cu^{2+}. At lower expression levels and intracellular concentrations of hSOD1 (~40 μM) and CCS (~15 μM), the authors detected complete disulfide bond formation of E,Zn-hSOD1^{S-S}, which suggested that this process also occurred independently of copper binding. Together, these data provided the first atomic-resolution insights into the maturation process of a human protein in a close-to-native intracellular environment.

Danielsson et al. (25) concurrently presented a similar in-cell NMR study on hSOD1 in human HeLa cells. In contrast to Banci et al. (11), these authors did not use sample overexpression and in-cell NMR measurements within the same cell type but instead delivered exogenously produced and isotope-labeled hSOD1 via the CPP tagging, protein transduction approach (42). Although hSOD1 overexpression yielded high quality in-cell NMR spectra in human HEK293T cells (11), transduction of homodimeric, full-length SOD1 into human HeLa cells was not achieved. Similar negative results were obtained with a monomeric, enzymatically active variant of SOD1, i.e., holoSOD1^{pwt}. Even a fully alanine-substituted, cysteine-depleted mutant, i.e., apo-hSOD1^{CallA}, was not internalized, collectively demonstrating that the efficiency of CPP-mediated protein delivery varies greatly between different cargos, even when they constitute different versions of the same protein.

Although not all mechanistic aspects of CPP-dependent intracellular protein delivery are well understood, positive net charges of the to-be-delivered CPP-cargo moieties are believed to be instrumental for efficient membrane crossing. Because hSOD1^{pwt} has a negative net charge only partially ameliorated by the presence of the eight-arginine CPP tag (the net charge of R8-hSOD1^{pwt} is ~0), Danielsson et al. (25) reasoned that removing hSOD1 active site loops IV and VII (i.e., hSOD1$^{\Delta IV\Delta VII}$) and changing the net charge to +5.4 might improve CPP-mediated cellular uptake. This was indeed the case. Consequently, in-cell NMR spectra of this hSOD1 mutant were of good quality and displayed well-dispersed resonance cross-peaks of folded hSOD1$^{\Delta IV\Delta VII}$. The chemically distinct CPP tag HIV-Tat gave similar results. In-cell NMR spectra revealed that hSOD1$^{\Delta IV\Delta VII}$ histidines were protonated, suggesting low pH conditions (~6.2) and considerable acidification of the HeLa cell cytoplasm, likely caused by metabolic ATP hydrolysis and oxygen deprivation when the growth medium is not replenished.

Indeed, nutrient depletion and metabolic exhaustion prompted Kubo et al. (52) to develop a miniature bioreactor for in-cell NMR applications in mammalian cells. In their setup, human HeLa S3 cells, grown in suspension, were targeted with isotope-labeled CAP-Gly1 (CG1, pI 5.2), the 9-kDa microtubule (MT)-binding domain of the human CLIP-170 protein, using the pore-forming bacterial toxin SLO (71). Cells were immobilized in a liquid three-dimensional matrix biogel solidified in a modified flow-cell NMR probe. Continuous media exchange ensured optimal control over metabolic parameters, such as intracellular ATP and pH, improving the overall quality of CG1 in-cell NMR spectra and leading to a substantial reduction in protein leakage (14). The authors subsequently recorded ^{1}H-^{13}C-methyl-TROSY in-cell NMR spectra over extended periods of time without sample deterioration (52). Their bioreactor setup also enabled in-cell transferred cross-saturation experiments between delivered, isotope-labeled CG1 and endogenous HeLa MTs. Results from these experiments confirmed that the same set of CG1 residues that interacted with MTs in vitro also bound to MTs in mammalian cells (52). A similar bioreactor setup was introduced for in-cell NMR measurements in bacteria (91).

Besides hSOD1, Banci et al. (11, 12) examined four other folded human proteins in human HEK293T cells: the mitochondrial intermembrane space importer and assembly protein 40 (Mia40, ~16 kDa, pI 4.0), glutaredoxin-1 (Grx1, ~12 kDa, pI 7.9), thioredoxin (Trx, ~12 kDa, pI 4.6), and the copper transporter Atox1 (~7.5 kDa, pI 7.0). Whereas all proteins were overexpressed to comparable intracellular levels, only Mia40 and Atox1 yielded interpretable in-cell NMR spectra. Grx1 and Trx1 remained invisible in intact cells and were detected only upon cell lysis. In-cell NMR studies of Atox1 binding to the anticancer drug cisplatin in bacteria were previously reported by the same group (2). Given these proteins' different sizes and overall net charges, no clear correlations between their in-cell NMR behaviors and general physical properties could be established.

Upon Mia40 overexpression in mammalian cells, in-cell NMR measurements revealed that the protein was predominantly cytoplasmic and remained in its fully oxidized, folded state despite the reducing cytoplasmic environment (12), indicating that high levels of endogenous agents, such as glutathione, did not reduce the protein. Because Grx1 and Trx1 are cytoplasmic oxidoreductases that also control cellular thiol homeostasis, Banci et al. (12) co-overexpressed Mia40 with Grx1. In-cell NMR spectra showed that under these conditions, Mia40 was mostly unfolded and reduced, whereas co-overexpression with Trx1 had a smaller effect. In contrast to what was observed in intact cells, increasing amounts of fully reduced Grx1 had no effect on the redox state of $Mia40^{2S-S}$ when both proteins were reacted in vitro in the presence of dithiothreitol or reduced glutathione. These results excluded a mechanistic notion that Grx1 was directly involved in the reduction of $Mia40^{2S-S}$. They also suggested that cellular activities other than Grx1 alone were required to maintain cytoplasmic Mia40 in its reduced form in vivo. Yet again, these conclusions underscore the tremendous biological impacts that simple in-cell NMR measurements can have.

In-Cell NMR of DNA and RNA

The advent of in-cell NMR applications in *X. laevis* oocytes and targeted delivery of isotope-labeled proteins by microinjection also spurred in-cell NMR studies of nucleic acids (NAs) (36–38, reviewed in 35). Initially, isotope-labeled DNA and RNA hairpins were injected into *Xenopus* oocytes, and 2-D ^{1}H-^{13}C correlation experiments were recorded over ~20 h (36). Site-specific exo- and endonuclease cleavage of the DNA hairpin was observed after 5 h—which eventually led to the production of single nucleotides—but the RNA hairpin proved to be more stable. However, it was more prone to nonspecific interactions with cellular components, which similarly diminished specific NMR signals over time. Synthetic incorporation of noncleavable phosphorothioate bonds in the two hairpins and methylation of the RNA O2′-hydroxyls rendered both structures nuclease-resistant. This indicates that high-resolution in-cell NMR studies of unmodified DNA and RNA hairpins are feasible within a time window of 2–5 h, whereas modified NAs can be analyzed over extended periods of time. Hänsel et al. (36) further showed that the 1-D ^{1}H region between 11.0 and 14.0 ppm of intact *Xenopus* oocytes, corresponding to the imino-proton region of NAs, is devoid of background proton signals. Therefore, qualitative in-cell NMR experiments can also be performed on non-^{13}C- or ^{15}N-isotope-labeled, injected NA samples, by exploiting their NMR-active proton signals only.

The human telomeric repeat sequence $d(G_3(TTAG_3)_3T)$ was the first guanine-rich NA quadruplex (G-quadruplex) structure to be investigated by in-cell NMR (36). G-quadruplexes form at the 3′ end of vertebrate chromosomes, where thousands of tandem repeats of the G-rich sequence $(GGGTTA)_n$ constitute the chromosomal end structures called telomeres. Many in vitro studies of various telomeric four-G-repeat sequences indicated that their folding topologies greatly depend on the experimental conditions employed for their characterization. Factors that

modulate G-quadruplex structures in vitro include sequence composition, the presence and type of counterions, and the degree of macromolecular crowding.

Whereas the 1-D proton spectrum of unlabeled, isolated $d(G_3(TTAG_3)_3T)$ confirmed the presence of the two-tetrad antiparallel basket-type G-quadruplex structure, Hänsel et al. (36) obtained a strikingly different imino-proton envelope in intact *Xenopus* oocytes that suggested alternative conformations inside these cells. Upon oocyte lysis, mixed populations of basket- and nonbasket-type structures were detected and quantitatively converted into the original topology when precipitated with butanol and resuspended in NMR buffer (36). A similar study in polyethylene glycol (PEG)- and Ficoll-crowded in vitro solutions showed that the structural properties of $TAG_3(TTAG_3)_3$, i.e., TA-core, and $AG_3(TTAG_3)_3TT$, i.e., A-core TT G-quadruplex, were substantially different than in *Xenopus* cytostatic factor (CSF)-arrested eggs extracts (37). Whereas crowding with PEG induced stacking of preferentially parallel G-quadruplex conformations, crowding with Ficoll preserved unimolecular conformations also found in dilute potassium solutions. Interestingly, G-quadruplexes in CSF extracts displayed varying degrees of structural heterogeneity that corresponded to superpositions of the original hybrid and alternative conformations, potentially resembling the parallel topology obtained in PEG environments. This argues that mixed populations of interconverting conformers exist in physiological solutions. To increase spectral resolution under cellular conditions, Hänsel et al. (38) employed 2-D ^{1}H-^{15}N correlation NMR experiments and ^{15}N-^{13}C isotope-labeled $d(AG_3(TTAG_3)_3)$ to demonstrate that the *Xenopus* CSF extract-folded G-quadruplex exhibited the hybrid-1 topology, which is also prominently populated in dilute potassium solutions.

In-Cell EPR

In-cell NMR work on proteins and G-quadruplex structures in *X. laevis* oocytes also led to the development of novel pulsed-field electron paramagnetic resonance (EPR) and double electron-electron resonance (PELDOR or DEER) spectroscopy applications, in combination with site-directed spin labeling (SDSL) in this particular cell type (5–8, 41, 51). EPR and DEER applications are advantageous in that they provide long-range distance information (1.5 to 8 nm) between unpaired electron spin centers introduced into proteins or NAs. This broad range of measurable distances is comparable to Förster resonance energy transfer (FRET) techniques. One major obstacle to EPR applications in live cells is the difficulty of generating spin labels that bear no reducible protein/NA linkages and thus can withstand the reducing environment of the intracellular space (5, 41, 51). In their pilot DEER study in *Xenopus* oocytes, Igarashi et al. (41) used maleimide conjugation instead of disulfide coupling to introduce stable spin labels (nitroxide-based 3-maleimido-PROXYL) at three Ub positions to comparatively analyze intramolecular distances in dilute in vitro solutions and intact cells. Sample delivery by microinjection and in-cell DEER measurements yielded comparable distances between the individual spin centers in both environments, which collectively suggested that the global folding topology of this small protein is preserved in the intracellular space of *Xenopus* oocytes. The data from Igarashi et al. (41) also indicated that the employed nitroxide radicals had limited lifetimes (~1 h) and presumably succumbed to reductive conversion and the formation of EPR-silent hydroxylamines, thus illustrating the need for spin labels with longer half-lives in physiological environments.

Azarkh et al. (5) and Krstić et al. (51) investigated the cellular lifetimes of different spin labels in more detail and found that chemically similar probes were reduced at different rates in *Xenopus* CSF extracts, which, the authors argued, supported the notion that intracellular nitroxide reduction constituted an enzyme-mediated process. The Drescher group (6) and Krstić et al. (51) investigated complementary double-stranded and spin-labeled DNA 7- and 12-mers in *Xenopus*

^{19}F IN-CELL NMR

^{19}F-labeled proteins are becoming increasingly important for in-cell NMR applications (56, 57, 61, 92, 104, 108, 109). ^{19}F bears several advantages as it has a spin quantum number of 1/2, rendering NMR detection straightforward. With a gyromagnetic ratio (γ_n) that is 83% that of a proton, ^{19}F is a highly sensitive nucleus, and its spectral simplicity and large chemical shift range are attractive for protein-based applications. Site-selective ^{19}F isotopic labeling of tryptophan, tyrosine, or phenylalanine side chains can be achieved via incorporation of orthogonal aminoacyl-tRNA synthetase/tRNA pairs and unnatural amino acids at engineered amber codon sites (60). This method was first employed in 2007 to produce site-selective, ^{19}F-labeled proteins for structural studies (34, 45). Simpler and more economical ^{19}F labeling of tryptophan is accomplished by recombinant protein expression in 5-fluoroindole-containing growth media (23).

oocytes, respectively. The shorter 7-mer displayed comparable in vitro and in-cell DEER distances between the engineered spin pairs, although with a broader in-cell distance distribution, possibly caused by partial DNA melting (6). In-cell DEER measurements of the longer and less A-T-rich 12-mer revealed a superposition of mixed distance states (51). One of these states was attributed to the monomeric DNA duplex conformation with in-cell DEER distances that deviated little from in vitro measurements; the other originated from an end-to-end duplex stacking topology, a well-known phenomenon of double-stranded DNA of this size. Together, these data demonstrated that short, double-stranded, B-form DNA retains its conformation inside live oocyte cells.

Krstić et al. (51) further characterized in-cell distance properties of 14- and 27-mer RNA hairpin and riboswitch structures, respectively. Immediately after oocyte injection, DEER measurements revealed fast transverse relaxation rates that decreased considerably over time. The authors interpreted this behavior as reflecting high initial spin concentrations following the injection process that progressively weakened because of intracellular diffusion and spin-label reduction. Overall, both RNA structures retained their in vitro conformations inside *Xenopus* oocytes, confirming the stability of these topologies under native cellular conditions.

Spin labels can also be used to complement and clarify structural insights from other methods. As an example, we return to where we left off in the in-cell NMR study of the d($AG_3(TTAG_3)_3$) G-quadruplex, which was also investigated in a site-selective, spin-labeled form with in-cell DEER methods (7). In contrast to in-cell NMR– and fluorescence-derived data [which point to hybrid-1 conformations in *Xenopus* oocytes, egg extracts, and potassium solutions at physiological temperatures (38)], results from in-cell DEER measurements at cryogenic temperatures suggested that d($AG_3(TTAG_3)_3$) coexists in three-tetrad antiparallel basket and parallel propeller structures; these were previously found in dilute potassium solutions (94). When Hänsel et al. (38) compared in-cell and in vitro measured distances between spin label–modified thymidines in d($AG_3(TTAG_3)_3$) and in silico–derived reference distances from X-ray and NMR G-quadruplex structures, they could not unambiguously distinguish between parallel propeller, three-tetrad antiparallel basket, and hybrid-1 structures because of the poor definition of thymine positions in the previously calculated NMR ensembles.

SOLID-STATE IN-CELL NMR

The requirement for fast rotational tumbling of biomolecules is one major limitation of solution-state in-cell NMR applications. Although bulk intracellular solvent viscosity is only approximately twice that of dilute buffers in most cells, weak and nonspecific interactions with cellular components

often hamper in-cell NMR measurements. Efforts to overcome these detrimental effects include detection of in-cell ^{13}C-methyl side-chain resonances or the use of ^{19}F NMR (see Sidebar, ^{19}F In-Cell NMR). In many instances, however, researchers wish to study large macromolecular assemblies or membrane proteins, which necessitate different approaches. High-resolution magic angle spinning (HR-MAS) solid-state NMR methods on cellular samples have been successfully employed to this end (74, 78). Introduced in 2001 to characterize the abundant osmoregulated periplasmic glucans in *Ralstonia solanacearum* (103), HR-MAS methods have since been used to study protein structures in bacterial inclusion bodies (24, 102), intracellular protein assemblies (77), membrane proteins in isolated membranes (32, 46, 48, 58, 79, 80), and whole cells (47, 80, 99, 105). Some of these on-cell NMR studies are discussed in Solution-State On-Cell NMR, below. Of particular note, recent HR-MAS solid-state NMR applications on cellular preparations have used dynamic nuclear polarization (DNP) enhancement, which, in principle, should greatly improve sensitivity and make in-cell NMR studies of native membrane systems feasible (46, 58, 79, 99).

SOLUTION-STATE ON-CELL NMR

The power of NMR to provide atomic-resolution insights into physiological processes inside cells is remarkable. However, many biomolecules function on the cell surface, and a different approach is required to study their structures. To analyze cell-surface molecules under physiological conditions, different solution- and solid-state on-cell NMR methods have been developed. Because the protein, lipid, and carbohydrate compositions of individual cells change continuously in response to internal and external cues, analyses of these compositions offer important clues toward metabolic cell states, genetic variations, or environmental perturbations.

Capsular polysaccharides (PSs) are crucial virulence factors on the surface of gram-negative bacteria. Once isolated and purified, these PSs are administered as vaccines to protect against a host of bacterial infections from organisms such as *Meningococcus*, *Pneumococcus*, and *Haemophilus*. For *E. coli* K1 and *Neisseria meningitidis* serogroup B, capsular PSs elicit a weaker immune response than PSs from other gram-negative bacteria. Interestingly, these two bacteria have the same capsular PS: $\alpha(2 \rightarrow 8)$ polysialic acid (PSA).

Many researchers have suggested that the weaker immunogenicity of $\alpha(2 \rightarrow 8)$ PSA is caused by the formation of lactones or by structural changes that may occur during isolation and purification. Azurmendi et al. (9) investigated $\alpha(2 \rightarrow 8)$ PSA on live bacteria and compared it to isolated and purified $\alpha(2 \rightarrow 8)$ PSA by supplying *E. coli* with ^{15}N/^{13}C uniformly labeled sialic acid monomers. The mutant strain of *E. coli* used in this study was genetically engineered so that it could not metabolize sialic acid. Rather, the labeled monomers were incorporated as building blocks in the $\alpha(2 \rightarrow 8)$ polymer. Labeled $\alpha(2 \rightarrow 8)$ PSA was the dominant signal in 2-D NMR spectra without background interference from other biopolymers such as lipids, proteins, and NAs. Thus, NMR was used to examine the structure of $\alpha(2 \rightarrow 8)$ PSA on intact cells and to show that it did not contain detectable amounts of lactones. Nevertheless, subsequent on-cell NMR studies used a newly developed NMR pulse sequence to show evidence of lactones in low abundance (12a). These studies demonstrate that the development of novel NMR methods aimed at delineating details inside live cells could yield new information. In addition to these details, the original on-cell NMR spectra also allowed the authors to determine that 50% of the monomers had been converted to $\alpha(2 \rightarrow 8)$ PSA when spectra were acquired.

In addition to investigations of cell-surface PSs, many solution-state saturation-transfer difference and transferred nuclear Overhauser effect NMR experiments have been performed to characterize peptide interactions with cell-surface proteins on intact mammalian cells (3, 19, 63, 64, 75, 76).

SOLID-STATE ON-CELL NMR

Because structural modifications change glycan chemical shifts, on-cell NMR studies of glycans are used to determine their physiological structures. In particular, solid-state on-cell NMR experiments were successfully employed to analyze cell-surface glycans and to follow biologically relevant processes that alter their composition and conformation (28, 47, 48, 106, 107). In 1999, Jachymek et al. (44) used solid-state on-cell NMR applications to determine the structural differences among O-polysaccharide (O-PS) antigens of four strains of *Yokenella regensburgei*. NMR spectra of these isolated O-PSs were obtained on intact bacteria. This work showed that the O-PS backbone was the same for each strain [→3)-α-D-Fuc*p*NAc-(1→2)–L-α-D-Hep*p*-(1→3)-6-deoxy-α-L-Tal*p*-(1→], but it displayed different degrees of O-acetylation: PCM 2476 was O-acetylated at positions C2 and C4 of the deoxytallose moiety, whereas PCM 2477, 2478, and 2494 were O-acetylated only at the C2 position. Correspondingly, O-PSs from PCM 2477, 2478, and 2494 were recognized by one antibody, whereas PCM 2476 reacted with a different antibody. These differences in O-PS acetylation patterns have important ramifications for vaccine design.

In another on-cell NMR study, Zandomeneghi et al. (105) examined changes in O-PS compositions during the four growth phases—lag, exponential growth, stationary, and death—of *Salmonella enterica*, the pathogen that causes gastroenteritis. They showed that O-acetylation of the major [→2)-α-D-Man*p*-(1→4)–α-L-Rha*p*-(1→3)-α-D-Gal*p*-(1→] antigen changed significantly over time, and this may be directly linked to differences in its immunogenicity. The authors noted that de-O-acetylation spontaneously occurred when the pH of the continuously grown cultures increased, whereas O-acetylation levels remained constant when growth conditions were kept artificially acidic. As before, these findings also have a direct impact on vaccine development.

Other glycans such as peptidoglycan (PG) are important structural elements of outer bacterial cell walls. PG consists of linear glycan chains cross-linked by short tetrapeptides. The glycan chains are repeating disaccharide units of *N*-acetyl glucosamine linked β-1→4 to *N*-acetyl muramic acid. Many antibiotics target PG and interfere with a bacterium's ability to resist external mechanical stress. Therefore, on-cell NMR studies of drug-PG interactions are very likely to improve rational drug design.

Indeed, physiological structure–activity relationship studies underscore the great value of on-cell NMR approaches in aiding the drug design process. In one study, Kim & Schaefer (49) used solid-state on-cell NMR methods to delineate the mechanisms of substituted chloroeremomycin interactions with vancomycin-resistant enterococci and *Staphylococcus aureus*. These authors investigated the on-cell structures of two antibiotic-PG complexes and correlated these with different inhibitory activities. The antibiotics—*N*-(4-fluorobenzyl)vancomycin (FBV) and *N*-(4-(4-fluorophenyl)benzyl)vancomycin (FPBV)—had different hydrophobic side-chain lengths and therefore differed in their interactions with PG. To verify this, *S. aureus* cultures were grown in D-[1-^{13}C]-alanine–, [1-^{13}C]-glycine–, or L-[ε-^{15}N]-lysine–supplemented growth media, and internuclear distances between ^{19}F fluorine–substituted FBV and FPBV and between ^{13}C- or ^{15}N-isotope-labeled PG were measured. On-cell rotational-echo double resonance (REDOR) NMR experiments showed that FBV engaged in fewer PG contacts than FPBV and displayed higher conformational heterogeneity, which translated into its reduced antimicrobial activity. Work in a similar vein delineated the mechanisms of action of vancomycin and oritavancin on intact *Enterococcus faecium* cells. On-cell REDOR experiments showed that the two antibiotics bound PG differently and exhibited accordingly different modes of antimicrobial action (72). In another study, Kim et al. (50) demonstrated that oritavancin bound to isolated *S. aureus* protoplast membranes but not to intact protoplasts. On-cell NMR studies offer great hope for assisting in designing new therapies.

SUMMARY POINTS

1. Proteins engage in nonspecific and weak interactions with different cellular components. The range and magnitude of these interactions are protein-specific and depend on biological activity and on electrostatic and hydrophobic surface properties.
2. Different proteins experience different degrees of nonspecific interactions in different cellular and subcellular environments. These interactions affect their in-cell NMR behaviors.
3. Soft interactions often supersede purely physical, hard-sphere repulsions and must be taken into account in discussions of the cellular aspects and consequences of macromolecular crowding and excluded volume effects (83).
4. Artificial crowding reagents such as Ficoll and PEG do not recapitulate the full range of biological contributions that proteins experience inside cells (31). Therefore, appropriate cellular model systems and direct in situ approaches should be employed to study these effects.
5. Soft interactions also likely contribute to the structural and functional properties of other intra- and extracellular biomolecules, including NAs, lipids, and glycans.
6. Cellular processes such as posttranslational modifications, redox reactions, processing and maturation events, and metal binding dynamically alter the chemical, structural, and functional properties of biomolecules in and on cells. These changes reflect important physiological properties that must be taken into account when defining a molecule's biological activity.

FUTURE ISSUES

1. Given the range of established prokaryotic and eukaryotic in- and on-cell NMR systems, future studies should be carried out in the most physiologically relevant cellular environment rather than the most accessible one.
2. The development of a cheap, robust, and generic procedure to generate mammalian in-cell NMR samples is highly desirable.
3. Live cell NMR applications should employ experimental setups that ensure stable and controllable environmental and metabolic conditions for in- and on-cell NMR measurements. High-sensitivity NMR flow probes with built-in bioreactors for growing different cell types are an important next step in hardware development.

DISCLOSURE STATEMENT

The authors are not aware of any affiliations, memberships, funding, or financial holdings that might be perceived as affecting the objectivity of this review.

ACKNOWLEDGMENTS

All isoelectric points (pI) given in this review were recalculated with the 2007–2012 Isoelectric Point Calculator by L. Kozlowski (**http://isoelectric.ovh.org**), which provides theoretical

values based on multiple algorithms. Numbers represent average pI values according to protein sequence information listed in the original publications. We thank Gary Pielak, Lucia Banci, Enrico Luchinat, Robert Hänsel, Lukáš Trantírek, Mikael Oliveberg, and Jens Danielsson for carefully reading individual sections of the manuscript and for providing helpful feedback. This work was supported by an Emmy Noether program grant (SE-1794/1-1) by the Deutsche Forschungsgemeinschaft (DFG) to P.S.

LITERATURE CITED

1. Amata I, Maffei M, Igea A, Gay M, Vilaseca M, et al. 2013. Multi-phosphorylation of the intrinsically disordered unique domain of c-Src studied by in-cell and real-time NMR spectroscopy. *ChemBioChem*. 14:1820–27
2. Arnesano F, Banci L, Bertini I, Felli IC, Losacco M, Natile G. 2011. Probing the interaction of cisplatin with the human copper chaperone Atox1 by solution and in-cell NMR spectroscopy. *J. Am. Chem. Soc.* 133:18361–69
3. Assadi-Porter FM, Tonelli M, Maillet E, Hallenga K, Benard O, et al. 2008. Direct NMR detection of the binding of functional ligands to the human sweet receptor, a heterodimeric family 3 GPCR. *J. Am. Chem. Soc.* 130:7212–13
4. Augustus AM, Reardon PN, Spicer LD. 2009. MetJ repressor interactions with DNA probed by in-cell NMR. *Proc. Natl. Acad. Sci. USA* 106:5065–69
5. Azarkh M, Okle O, Eyring P, Dietrich DR, Drescher M. 2011. Evaluation of spin labels for in-cell EPR by analysis of nitroxide reduction in cell extract of *Xenopus laevis* oocytes. *J. Magn. Reson.* 212:450–54
6. Azarkh M, Okle O, Singh V, Seemann IT, Hartig JS, et al. 2011. Long-range distance determination in a DNA model system inside *Xenopus laevis* oocytes by in-cell spin-label EPR. *ChemBioChem* 12:1992–95
7. Azarkh M, Singh V, Okle O, Dietrich DR, Hartig JS, Drescher M. 2012. Intracellular conformations of human telomeric quadruplexes studied by electron paramagnetic resonance spectroscopy. *ChemPhysChem* 13:1444–47
8. Azarkh M, Singh V, Okle O, Seemann IT, Dietrich DR, et al. 2013. Site-directed spin-labeling of nucleotides and the use of in-cell EPR to determine long-range distances in a biologically relevant environment. *Nat. Protoc.* 8:131–47
9. Azurmendi HF, Vionnet J, Wrightson L, Trinh LB, Shiloach J, Freedberg DI. 2007. Extracellular structure of polysialic acid explored by on cell solution NMR. *Proc. Natl. Acad. Sci. USA* 104:11557–61
10. Banci L, Barbieri L, Bertini I, Cantini F, Luchinat E. 2011. In-cell NMR in *E. coli* to monitor maturation steps of hSOD1. *PLoS ONE* 6:e23561

11. First in-cell NMR study in human cells using protein overexpression; maturation of hSOD1 depended on the availability of different metals.

11. Banci L, Barbieri L, Bertini I, Luchinat E, Secci E, et al. 2013. Atomic-resolution monitoring of protein maturation in live human cells by NMR. *Nat. Chem. Biol.* 9:297–99

12. Banci L, Barbieri L, Luchinat E, Secci E. 2013. Visualization of redox-controlled protein fold in living cells. *Chem. Biol.* 20:747–52

12a. Barb AW, Freedberg DI, Battistel MD, Prestegard JH. 2011. NMR detection and characterization of sialylated glycoproteins and cell surface polysaccharides. *J. Biomol. NMR* 51:163–71

13. Barnes CO, Monteith WB, Pielak GJ. 2011. Internal and global protein motion assessed with a fusion construct and in-cell NMR spectroscopy. *ChemBioChem* 12:390–91
14. Barnes CO, Pielak GJ. 2011. In-cell protein NMR and protein leakage. *Proteins* 79:347–51
15. Benton LA, Smith AE, Young GB, Pielak GJ. 2012. Unexpected effects of macromolecular crowding on protein stability. *Biochemistry* 51:9773–75

16. First protein in-cell NMR study in yeast; spectral quality correlated with intracellular localization.

16. Bertrand K, Reverdatto S, Burz DS, Zitomer R, Shekhtman A. 2012. Structure of proteins in eukaryotic compartments. *J. Am. Chem. Soc.* 134:12798–806

17. Bodart J-F, Wieruszeski J-M, Amniai L, Leroy A, Landrieu I, et al. 2008. NMR observation of Tau in *Xenopus* oocytes. *J. Magn. Reson.* 192:252–57
18. Burz DS, Dutta K, Cowburn D, Shekhtman A. 2006. Mapping structural interactions using in-cell NMR spectroscopy (STINT-NMR). *Nat. Methods* 3:91–93

19. Claasen B, Axmann M, Meinecke R, Meyer B. 2005. Direct observation of ligand binding to membrane proteins in living cells by a saturation transfer double difference (STDD) NMR spectroscopy method shows a significantly higher affinity of integrin $\alpha_{IIb}\beta_3$ in native platelets than in liposomes. *J. Am. Chem. Soc.* 127:916–19
20. Costa JL, Dobson CM, Kirk KL, Poulsen FM, Valeri CR, Vecchione JJ. 1979. Studies of human platelets by ^{19}F and ^{31}P NMR. *FEBS Lett.* 99:141–46
21. Costa JL, Dobson CM, Kirk KL, Poulsen FM, Valeri CR, Vecchione JJ. 1980. Nuclear magnetic resonance studies of blood platelets. *Philos. Trans. R. Soc. Lond. B* 289:413–23
22. Crowley PB, Chow E, Papkovskaia T. 2011. Protein interactions in the *Escherichia coli* cytosol: an impediment to in-cell NMR spectroscopy. *ChemBioChem* 12:1043–48
23. Crowley PB, Kyne C, Monteith WB. 2012. Simple and inexpensive incorporation of ^{19}F-tryptophan for protein NMR spectroscopy. *Chem. Commun.* 48:10681–83
24. Curtis-Fisk J, Spencer RM, Weliky DP. 2008. Native conformation at specific residues in recombinant inclusion body protein in whole cells determined with solid-state NMR spectroscopy. *J. Am. Chem. Soc.* 130:12568–69
25. Danielsson J, Inomata K, Murayama S, Tochio H, Lang L, et al. 2013. Pruning the ALS-associated protein SOD1 for in-cell NMR. *J. Am. Chem. Soc.* 135:10266–69
26. Deeds EJ, Ashenberg O, Shakhnovich EI. 2006. A simple physical model for scaling in protein-protein interaction networks. *Proc. Natl. Acad. Sci. USA* 103:311–16
27. Deszo EL, Steenbergen SM, Freedberg DI, Vimr ER. 2005. *Escherichia coli* K1 polysialic acid *O*-acetyltransferase gene, *neuO*, and the mechanism of capsule form variation involving a mobile contingency locus. *Proc. Natl. Acad. Sci. USA* 102:5564–69
28. Dick-Pérez M, Zhang Y, Hayes J, Salazar A, Zabotina OA, Hong M. 2011. Structure and interactions of plant cell-wall polysaccharides by two- and three-dimensional magic-angle-spinning solid-state NMR. *Biochemistry* 50:989–1000
29. Ellis RJ. 2001. Macromolecular crowding: an important but neglected aspect of the intracellular environment. *Curr. Opin. Struct. Biol.* 11:114–19
30. Ellis RJ. 2001. Macromolecular crowding: obvious but underappreciated. *Trends Biochem. Sci.* 26:597–604
31. Feig M, Sugita Y. 2012. Variable interactions between protein crowders and biomolecular solutes are important in understanding cellular crowding. *J. Phys. Chem. B* 116:599–605
32. Fu R, Wang X, Li C, Santiago-Miranda AN, Pielak GJ, Tian F. 2011. In situ structural characterization of a recombinant protein in native *Escherichia coli* membranes with solid-state magic-angle-spinning NMR. *J. Am. Chem. Soc.* 133:12370–73
33. Hamatsu J, O'Donovan D, Tanaka T, Shirai T, Hourai Y, et al. 2013. High-resolution heteronuclear multidimensional NMR of proteins in living insect cells using a baculovirus protein expression system. *J. Am. Chem. Soc.* 135:1688–91
34. Hammill JT, Miyake-Stoner S, Hazen JL, Jackson JC, Mehl RA. 2007. Preparation of site-specifically labeled fluorinated proteins for ^{19}F-NMR structural characterization. *Nat. Protoc.* 2:2601–7
35. Hänsel R, Foldynová-Trantírková S, Dötsch V, Trantírek L. 2013. Investigation of quadruplex structure under physiological conditions using in-cell NMR. *Top. Curr. Chem.* 330:47–65
36. Hänsel R, Foldynová-Trantírková S, Löhr F, Buck J, Bongartz E, et al. 2009. Evaluation of parameters critical for observing nucleic acids inside living *Xenopus laevis* oocytes by in-cell NMR spectroscopy. *J. Am. Chem. Soc.* 131:15761–68
37. Hänsel R, Löhr F, Foldynová-Trantírková S, Bamberg E, Trantírek L, Dötsch V. 2011. The parallel G-quadruplex structure of vertebrate telomeric repeat sequences is not the preferred folding topology under physiological conditions. *Nucleic Acids Res.* 39:5768–75
38. Hänsel R, Löhr F, Trantírek L, Dötsch V. 2013. High-resolution insight into G-overhang architecture. *J. Am. Chem. Soc.* 135:2816–24
39. Heo M, Maslov S, Shakhnovich E. 2011. Topology of protein interaction network shapes protein abundances and strengths of their functional and nonspecific interactions. *Proc. Natl. Acad. Sci. USA* 108:4258–63

33. First protein in-cell NMR study in insect Sf9 cells.

37. G-quadruplex structures in *Xenopus* oocytes were different from those in vitro topologies.

40. Holder IT, Drescher M, Hartig JS. 2013. Structural characterization of quadruplex DNA with in-cell EPR approaches. *Bioorganic Med. Chem.* 21:6156–61

41. First protein in-cell EPR study; spin-spin distance measurements showed that ubiquitin retained its overall folding topology.

41. Igarashi R, Sakai T, Hara H, Tenno T, Tanaka T, et al. 2010. Distance determination in proteins inside *Xenopus laevis* oocytes by double electron-electron resonance experiments. *J. Am. Chem. Soc.* 132:8228–29

42. Inomata K, Ohno A, Tochio H, Isogai S, Tenno T, et al. 2009. High-resolution multi-dimensional NMR spectroscopy of proteins in human cells. *Nature* 458:106–9

43. Ito Y, Selenko P. 2010. Cellular structural biology. *Curr. Opin. Struct. Biol.* 20:640–48

44. Jachymek W, Niedziela T, Petersson C, Lugowski C, Czaja J, Kenne L. 1999. Structures of the O-specific polysaccharides from *Yokenella regensburgei* (*Koserella trabulsii*) strains PCM 2476, 2477, 2478, and 2494: high-resolution magic-angle spinning NMR investigation of the O-specific polysaccharides in native lipopolysaccharides and directly on the surface of living bacteria. *Biochemistry* 38:11788–95

45. Jackson JC, Hammill JT, Mehl RA. 2007. Site-specific incorporation of a ^{19}F-amino acid into proteins as an NMR probe for characterizing protein structure and reactivity. *J. Am. Chem. Soc.* 129:1160–66

46. Jacso T, Franks WT, Rose H, Fink U, Broecker J, et al. 2012. Characterization of membrane proteins in isolated native cellular membranes by dynamic nuclear polarization solid-state NMR spectroscopy without purification and reconstitution. *Angew. Chem. Int. Ed.* 51:432–35

47. Kern T, Giffard M, Hediger S, Amoroso A, Giustini C, et al. 2010. Dynamics characterization of fully hydrated bacterial cell walls by solid-state NMR: evidence for cooperative binding of metal ions. *J. Am. Chem. Soc.* 132:10911–19

48. Kern T, Hediger S, Müller P, Giustini C, Joris B, et al. 2008. Toward the characterization of peptidoglycan structure and protein-peptidoglycan interactions by solid-state NMR spectroscopy. *J. Am. Chem. Soc.* 130:5618–19

49. Fluorinated antibiotics were localized in regions of partially labeled peptidoglycan using solid-state NMR REDOR experiments on cells.

49. Kim SJ, Schaefer J. 2008. Hydrophobic side-chain length determines activity and conformational heterogeneity of a vancomycin derivative bound to the cell wall of *Staphylococcus aureus*. *Biochemistry* 47:10155–61

50. Kim SJ, Singh M, Schaefer J. 2009. Oritavancin binds to isolated protoplast membranes but not intact protoplasts of *Staphylococcus aureus*. *J. Mol. Biol.* 391:414–25

51. Krstić I, Hänsel R, Romainczyk O, Engels JW, Dötsch V, Prisner TF. 2011. Long-range distance measurements on nucleic acids in cells by pulsed EPR spectroscopy. *Angew. Chem. Int. Ed.* 50:5070–74

52. Kubo S, Nishida N, Udagawa Y, Takarada O, Ogino S, Shimada I. 2013. A gel-encapsulated bioreactor system for NMR studies of protein-protein interactions in living mammalian cells. *Angew. Chem. Int. Ed.* 52:1208–11

53. Latham MP, Kay LE. 2012. Is buffer a good proxy for a crowded cell-like environment? A comparative NMR study of calmodulin side-chain dynamics in buffer and *E. coli* lysate. *PLoS ONE* 7:e48226

54. NMR studies of side-chain dynamics in bacterial cell extracts delineated different types of calmodulin interactions.

54. Latham MP, Kay LE. 2013. Probing nonspecific interactions of Ca^{2+}-calmodulin in *E. coli* lysate. *J. Biomol. NMR* 55:239–47

55. Li C, Liu M. 2013. Protein dynamics in living cells studied by in-cell NMR spectroscopy. *FEBS Lett.* 587:1008–11

56. Li C, Lutz EA, Slade KM, Ruf RA, Wang GF, Pielak GJ. 2009. ^{19}F NMR studies of α-synuclein conformation and fibrillation. *Biochemistry* 48:8578–84

57. Li C, Wang G-F, Wang Y, Creager-Allen R, Lutz EA, et al. 2010. Protein ^{19}F NMR in *Escherichia coli*. *J. Am. Chem. Soc.* 132:321–27

58. Linden AH, Lange S, Franks WT, Akbey U, Specker E, et al. 2011. Neurotoxin II bound to acetylcholine receptors in native membranes studied by dynamic nuclear polarization NMR. *J. Am. Chem. Soc.* 133:19266–69

59. Link AJ, Robison K, Church GM. 1997. Comparing the predicted and observed properties of proteins encoded in the genome of *Escherichia coli* K-12. *Electrophoresis* 18:1259–313

60. Liu CC, Schultz PG. 2010. Adding new chemistries to the genetic code. *Annu. Rev. Biochem.* 79:413–44

61. Liu JJ, Horst R, Katritch V, Stevens RC, Wuthrich K. 2012. Biased signaling pathways in β_2-adrenergic receptor characterized by ^{19}F-NMR. *Science* 335:1106–10

62. Maldonado AY, Burz DS, Shekhtman A. 2011. In-cell NMR spectroscopy. *Prog. Nucl. Magn. Reson. Spectrosc.* 59:197–212

63. Mari S, Invernizzi C, Spitaleri A, Alberici L, Ghitti M, et al. 2010. 2D TR-NOESY experiments interrogate and rank ligand-receptor interactions in living human cancer cells. *Angew. Chem. Int. Ed.* 49:1071–74
64. Mari S, Serrano-Gómez D, Cañada FJ, Corbí AL, Jiménez-Barbero J. 2004. 1D saturation transfer difference NMR experiments on living cells: the DC-SIGN/oligomannose interaction. *Angew. Chem. Int. Ed.* 44:296–98
65. Miklos AC, Li C, Sharaf NG, Pielak GJ. 2010. Volume exclusion and soft interaction effects on protein stability under crowded conditions. *Biochemistry* 49:6984–91
66. Miklos AC, Li C, Sorrell CD, Lyon LA, Pielak GJ. 2011. An upper limit for macromolecular crowding effects. *BMC Biophys.* 4:13
67. Miklos AC, Sarkar M, Wang Y, Pielak GJ. 2011. Protein crowding tunes protein stability. *J. Am. Chem. Soc.* 133:7116–20
68. Minton AP. 2000. Implications of macromolecular crowding for protein assembly. *Curr. Opin. Struct. Biol.* 10:34–39
69. Minton AP. 2001. The influence of macromolecular crowding and macromolecular confinement on biochemical reactions in physiological media. *J. Biol. Chem.* 276:10577–80
70. Minton AP. 2013. Quantitative assessment of the relative contributions of steric repulsion and chemical interactions to macromolecular crowding. *Biopolymers* 99:239–44
71. Ogino S, Kubo S, Umemoto R, Huang S, Nishida N, Shimada I. 2009. Observation of NMR signals from proteins introduced into living mammalian cells by reversible membrane permeabilization using a pore-forming toxin, streptolysin O. *J. Am. Chem. Soc.* 131:10834–35
72. Patti GJ, Kim SJ, Yu T-Y, Dietrich E, Tanaka KSE, et al. 2009. Vancomycin and oritavancin have different modes of action in *Enterococcus faecium*. *J. Mol. Biol.* 392:1178–91
73. Pielak GJ, Li C, Miklos AC, Schlesinger AP, Slade KM, et al. 2009. Protein nuclear magnetic resonance under physiological conditions. *Biochemistry* 48:226–34
74. Pielak GJ, Tian F. 2012. Membrane proteins, magic-angle spinning, and in-cell NMR. *Proc. Natl. Acad. Sci. USA* 109:4715–16
75. Potenza D, Belvisi L. 2008. Transferred-NOE NMR experiments on intact human platelets: receptor-bound conformation of RGD-peptide mimics. *Org. Biomol. Chem.* 6:258–62
76. Potenza D, Vasile F, Belvisi L, Civera M, Araldi EMV. 2011. STD and trNOESY NMR study of receptor-ligand interactions in living cancer cells. *ChemBioChem* 12:695–99
77. Reckel S, Lopez JJ, Löhr F, Glaubitz C, Dötsch V. 2012. In-cell solid-state NMR as a tool to study proteins in large complexes. *ChemBioChem* 13:534–37
78. Renault M, Cukkemane A, Baldus M. 2010. Solid-state NMR spectroscopy on complex biomolecules. *Angew. Chem. Int. Ed.* 49:8346–57
79. Renault M, Pawsey S, Bos MP, Koers EJ, Nand D, et al. 2012. Solid-state NMR spectroscopy on cellular preparations enhanced by dynamic nuclear polarization. *Angew. Chem. Int. Ed.* 51:2998–3001
80. Renault M, Tommassen-van Boxtel R, Bos MP, Post JA, Tommassen J, Baldus M. 2012. Cellular solid-state nuclear magnetic resonance spectroscopy. *Proc. Natl. Acad. Sci. USA* 109:4863–68
81. Sakai T, Tochio H, Inomata K, Sasaki Y, Tenno T, et al. 2007. Fluoroscopic assessment of protein leakage during *Xenopus* oocytes in-cell NMR experiment by co-injected EGFP. *Anal. Biochem.* 371:247–49
82. Sakai T, Tochio H, Tenno T, Ito Y, Kokubo T, et al. 2006. In-cell NMR spectroscopy of proteins inside *Xenopus* laevis oocytes. *J. Biomol. NMR* 36:179–88
83. Sarkar M, Li C, Pielak GJ. 2013. Soft interactions and crowding. *Biophys. Rev.* 1:1–8
84. Schlesinger AP, Wang Y, Tadeo X, Millet O, Pielak GJ. 2011. Macromolecular crowding fails to fold a globular protein in cells. *J. Am. Chem. Soc.* 133:8082–85
85. Selenko P, Frueh DP, Elsaesser SJ, Haas W, Gygi SP, Wagner G. 2008. In situ observation of protein phosphorylation by high-resolution NMR spectroscopy. *Nat. Struct. Mol. Biol.* 15:321–29
86. Selenko P, Serber Z, Gadea B, Ruderman J, Wagner G. 2006. Quantitative NMR analysis of the protein G B1 domain in *Xenopus laevis* egg extracts and intact oocytes. *Proc. Natl. Acad. Sci. USA* 103:11904–9
87. Serber Z, Corsini L, Durst F, Dötsch V. 2005. In-cell NMR spectroscopy. *Methods Enzymol.* 394:17–41
88. Serber Z, Keatinge-Clay AT, Ledwidge R, Kelly AE, Miller SM, Dötsch V. 2001. High-resolution macromolecular NMR spectroscopy inside living cells. *J. Am. Chem. Soc.* 123:2446–47

80. Benchmark solid-state on-cell NMR study of integral bacterial membrane proteins, endogenous periplasmic proteoglycans, and outer membrane lipopolysaccharides.

89. Serber Z, Ledwidge R, Miller SM, Dötsch V. 2001. Evaluation of parameters critical to observing proteins inside living *Escherichia coli* by in-cell NMR spectroscopy. *J. Am. Chem. Soc.* 123:8895–901
90. Serber Z, Selenko P, Hänsel R, Reckel S, Löhr F, et al. 2006. Investigating macromolecules inside cultured and injected cells by in-cell NMR spectroscopy. *Nat. Protoc.* 1:2701–9
91. Sharaf NG, Barnes CO, Charlton LM, Young GB, Pielak GJ. 2010. A bioreactor for in-cell protein NMR. *J. Magn. Reson.* 202:140–46
92. Shi P, Li D, Chen H, Xiong Y, Wang Y, Tian C. 2012. *In situ* ^{19}F NMR studies of an *E. coli* membrane protein. *Protein Sci.* 21:596–600
93. Shulman RG, Ogawa S, Mayer A, Castillo CL. 1973. High-resolution proton NMR studies of low affinity hemoglobins. *Ann. N.Y. Acad. Sci.* 222:9–20
94. Singh V, Azarkh M, Exner TE, Hartig JS, Drescher M. 2009. Human telomeric quadruplex conformations studied by pulsed EPR. *Angew. Chem. Int. Ed.* 48:9728–30
95. Slade KM, Baker R, Chua M, Thompson NL, Pielak GJ. 2009. Effects of recombinant protein expression on green fluorescent protein diffusion in *Escherichia coli*. *Biochemistry* 48:5083–89
96. Snyder GK. 1977. Blood corpuscles and blood hemoglobins: a possible example of coevolution. *Science* 195:412–13
97. Spitzer J, Poolman B. 2009. The role of biomacromolecular crowding, ionic strength, and physicochemical gradients in the complexities of life's emergence. *Microbiol. Mol. Biol. Rev.* 73:371–88
98. Tadeo X, López-Méndez B, Trigueros T, Laín A, Castaño D, Millet O. 2009. Structural basis for the aminoacid composition of proteins from halophilic archea. *PLoS Biol.* 7:e1000257
99. Takahashi H, Ayala I, Bardet M, De Paëpe G, Simorre J-P, Hediger S. 2013. Solid-state NMR on bacterial cells: selective cell wall signal enhancement and resolution improvement using dynamic nuclear polarization. *J. Am. Chem. Soc.* 135:5105–10
100. Wang Q, Zhuravleva A, Gierasch LM. 2011. Exploring weak, transient protein–protein interactions in crowded in vivo environments by in-cell nuclear magnetic resonance spectroscopy. *Biochemistry* 50:9225–36
101. Wang Y, Sarkar M, Smith AE, Krois AS, Pielak GJ. 2012. Macromolecular crowding and protein stability. *J. Am. Chem. Soc.* 134:16614–18
102. Wasmer C, Benkemoun L, Sabaté R, Steinmetz MO, Coulary-Salin B, et al. 2009. Solid-state NMR spectroscopy reveals that *E. coli* inclusion bodies of HET-s(218–289) are amyloids. *Angew. Chem. Int. Ed.* 48:4858–60
103. Wieruszeski JM, Bohin A, Bohin JP, Lippens G. 2001. *In vivo* detection of the cyclic osmoregulated periplasmic glucan of *Ralstonia solanacearum* by high-resolution magic angle spinning NMR. *J. Magn. Reson.* 151:118–23
104. Ye Y, Liu X, Zhang Z, Wu Q, Jiang B, et al. 2013. ^{19}F NMR spectroscopy as a probe of cytoplasmic viscosity and weak protein interactions in living cells. *Chem. Eur. J.* 19:12705–10
105. Zandomeneghi G, Ilg K, Aebi M, Meier BH. 2012. On-cell MAS NMR: physiological clues from living cells. *J. Am. Chem. Soc.* 134:17513–19
106. Zhong J, Frases S, Wang H, Casadevall A, Stark RE. 2008. Following fungal melanin biosynthesis with solid-state NMR: biopolymer molecular structures and possible connections to cell-wall polysaccharides. *Biochemistry* 47:4701–10
107. Zhou X, Cegelski L. 2012. Nutrient-dependent structural changes in *S. aureus* peptidoglycan revealed by solid-state NMR spectroscopy. *Biochemistry* 51:8143–53
108. Zigoneanu IG, Pielak GJ. 2012. Interaction of α-synuclein and a cell penetrating fusion peptide with higher eukaryotic cell membranes assessed by ^{19}F NMR. *Mol. Pharm.* 9:1024–29
109. Zigoneanu IG, Yang YJ, Krois AS, Haque E, Pielak GJ. 2012. Interaction of α-synuclein with vesicles that mimic mitochondrial membranes. *Biochim. Biophys. Acta* 1818:512–19

100. Comparative analysis of nonspecific protein interactions and their effects on in-cell NMR spectral quality in *E. coli*.

105. On-cell NMR analysis of changes in bacterial membrane composition during different growth stages.

Annual Review of Biophysics
Volume 43, 2014

Contents

Index

Errata

An online log of corrections to *Annual Review of Biophysics* articles may be found at http://www.annualreviews.org/errata/biophys